Available online at www.sciencedirect.com
ScienceDirect
C. R. Physique 10 (2009) 991–999
COMPTES RENDUS PHYSIQUE

Slow-light: Fascinating physics or potential applications?

Slow light using semiconductor optical amplifiers: Model and noise characteristics

Perrine Berger [a,b,*], Mehdi Alouini [c,a], Jérôme Bourderionnet [a], Fabien Bretenaker [b], Daniel Dolfi [a]

[a] *Thales Research & Technology, 1, avenue Augustin-Fresnel, 91767 Palaiseau cedex, France*
[b] *Laboratoire Aimé-Cotton, CNRS – université Paris Sud 11, campus d'Orsay, 91405 Orsay cedex, France*
[c] *Institut de physique de Rennes, UMR CNRS 6251, campus de Beaulieu, 35042 Rennes cedex, France*

Available online 31 December 2009

Abstract

We developed an improved model in order to predict the RF behavior of the SOA valid for any experimental conditions. It takes into account the dynamic saturation of the SOA, which can be fully characterized by a simple measurement, and only relies on material fitting parameters, independent of the optical intensity and bias current. We used this new model to analyze and model the additive noise of the SOA in order to fully characterize the influence of the slow light effect on the microwave photonics link properties. ***To cite this article: P. Berger et al., C. R. Physique 10 (2009).***

Résumé

Lumière lente dans les amplificateurs optiques à semi-conducteurs : Modélisation et caractérisation du bruit additif. Nous présentons un modèle amélioré prédisant la réponse RF de l'amplificateur optique à semi-conducteurs (SOA). Ce modèle reste valide quelles que soient les conditions expérimentales : en effet, il prend en compte la saturation dynamique du SOA, caractérisée par une expérience très simple, et ne repose que sur peu de paramètres d'ajustement, qui dépendent du matériau et non du courant d'injection ou de la puissance optique d'entrée. On utilise ce nouveau modèle pour caractériser le bruit additif du SOA, afin d'analyser les effets du ralentissement de la lumière sur les propriétés de la liaison opto-hyperfréquence. ***Pour citer cet article : P. Berger et al., C. R. Physique 10 (2009).***

Keywords: Slow light; Semiconductor optical amplifiers (SOA); Microwave photonics; Noise

Mots-clés : Lumière lente ; Amplificateur optique à semi-conducteurs (SOA) ; Opto-hyperfréquence ; Bruit

* Corresponding author at: Thales Research & Technology, 1, avenue Augustin-Fresnel, 91767 Palaiseau cedex, France.
E-mail address: perrine.berger@thalesgroup.com (P. Berger).

1631-0705/$ – see front matter
doi:10.1016/j.crhy.2009.10.005

1. Introduction

The control of the propagation velocity of optically carried microwave signals has been extensively studied over the past few years. The ability to generate continuously tunable delay lines can indeed now be readily implemented by electronic means. Slow light elements are therefore highly promising in the field of microwave photonics, with applications such as complex filtering of microwave signals, synchronization of optoelectronic oscillators, and control of optically fed phased array antennas [1–3]. Among the different slow light elements, one of the most mature approaches for integration in real field systems relies on Coherent Population Oscillations (CPO) in semiconductor structures [4–6]. This approach indeed offers compactness, continuous tunability of the delay through current injection and possible parallelism [7,8].

Numerous theoretical models describing the slow light effect in semiconductor amplifiers (SOAs) can be found in the literature [6,9–12]. They offer a comprehensive understanding of the slow light phenomena, the gain saturation dynamics and associated group index changes. On the one hand, a few theoretical models rely on a full description of the energy levels of the semiconductor structure [10,13], which are unfortunately usually not available when commercial SOAs are used. On the other hand, the slow light effect in SOAs is well explained by more practical models [6,14], but it is usually assumed that the saturation power and the carrier recombination lifetime are both constant along the propagation direction, by considering effective averaged parameters. These latter models thus become more phenomenological and fail to predict the SOA properties when the input optical power and the injected current vary over a large range.

However, a practical implementation of a semiconductor slow light element in a real microwave photonics link requires an accurate modeling of the impact of the component on the link performance. This includes gain and phase shifts caused by CPO, but also the ability of the link to transmit an analog RF signal without degrading its characteristics, which can be analyzed through the additive intensity noise and the dynamic range. Furthermore, since the generated delays are tuned by controlling the injected current and/or the optical input power, it is essential to have a reliable predictive model that can manage any change in these initial conditions.

In that frame, we propose in this paper an improved model that enables to accurately predict the RF gain compression and the RF phase delay. The adjustment parameters of our model are the material recombination coefficients, which are independent of experimental conditions, thus ensuring the predictive capability of the model for a given component. Furthermore, we show that this model is also efficient in describing the additional relative intensity noise of the SOAs.

2. Slow light properties in SOA

2.1. Model

We consider an optical carrier modulated by an RF signal and injected in a traveling wave SOA. The total field is then composed of the optical carrier of complex amplitude E_0 and two sidebands of complex amplitudes E_1 and E_2. Under the small RF signal approximation, we have $E_0 \gg E_1$, E_2, and the optical power inside the SOA can thus be written as $P = |E_{total}|^2 \times S_{guide} = P_0 + Me^{-i\Omega t} + \text{c.c.}$, where P_0 is the DC component of the power, and $M = (E_0 E_2^* + E_1 E_0^*) S_{guide}$ is the beat-note term at the RF frequency Ω. S_{guide} denotes the modal area of the SOA.

The local equations for the propagation of the optical fields and the evolution of carrier density inside the SOA lead to, for a small trench of SOA of thickness $\mathrm{d}z$ [9]:

$$\frac{\mathrm{d}P_0}{\mathrm{d}z} = P_0\big[-\gamma + \Gamma g(\bar{N})\big] \tag{1}$$

$$\frac{\mathrm{d}M}{\mathrm{d}z} = M\left[-\gamma + \Gamma g(\bar{N})\left(1 - \frac{P_0/P_s(\bar{N})}{1 + P_0/P_s(\bar{N}) - i\Omega\tau_s(\bar{N})}\right)\right] \tag{2}$$

where $\bar{N}$ is the steady state carrier density, γ holds for the internal losses of the SOA, and $\Gamma g(\bar{N})$ is the material modal gain. $\tau_s(\bar{N})$ is the carrier lifetime and $P_s(\bar{N})$ is the saturation power defined as: $P_s(\bar{N}) = \frac{\hbar\omega}{a(\bar{N})\tau_s(\bar{N})} S_{guide}$, where a is the differential gain $a = \frac{\partial g}{\partial N}|_{\bar{N}}$.

The common approach to solve Eqs. (1) and (2) is to consider a, τ_s and P_s constant with respect to the carrier density and thus over the whole length of the device [6]. Doing so, the system of equations can be analytically solved. However, in this case, the adjustment parameters τ_s and P_s vary with experimental conditions, and cannot be a priori estimated: the model thus becomes more phenomenological than predictive. Our focus in this article is to keep the predictive capability of the model. Consequently, we take into account the variations of a, τ_s, and therefore P_s, with respect to the carrier density modifications along the propagation axis. Our central hypothesis is that a and τ_s can be determined as functions of the DC component of the local optical power P_0 solely, allowing these dependencies to be determined from gain measurements.

The first step is to determine the variations of the modal gain Γg and of $\bar{N}/\tau_s$ as a function of the local DC optical power P_0. Consequently, a small signal gain measurement is conducted. It is understood by optical small signal that the injected optical power is lower than the SOA saturation optical power. If small signal conditions are fulfilled, the stimulated emission is negligible compared to the spontaneous emission, leading to the unsaturated steady state solution of the rate equation for the carriers:

$$\frac{I}{qLS_{act}} = \frac{\bar{N}}{\tau_s} \tag{3}$$

where L is the length of the SOA, S_{act} is the area of the active section of the SOA, and I the injected current. Moreover, if we also assume in this case that the carrier density $\bar{N}$ is constant along the SOA, a measurement of the small signal modal gain Γg_0 versus I will be equivalent, owing to Eq. (3), to a determination of the modal gain Γg versus $\bar{N}/\tau_s$. Here, Γ is the ratio S_{act}/S_{guide} of the active to modal gain areas in the SOA.

Combining this result with the saturated steady state solution of the carriers rate equation, one obtains the following set of equations:

$$\begin{aligned} &\frac{I}{qL} - S_{act}\frac{\bar{N}}{\tau_s} - \frac{\Gamma g(\frac{\bar{N}}{\tau_s})}{\hbar\omega}P_0 = 0 \\ &\Gamma g = \Gamma g(\bar{N}/\tau_s) \end{aligned} \tag{4}$$

By solving this set of equations, one obtains the variations of Γg and $\bar{N}/\tau_s$ versus P_0 and I, i.e., as a function of experimental parameters.

In order to get the differential gain and the carrier lifetime as well, an additional relation that enables to express $\bar{N}$ and τ_s as a function of $\bar{N}/\tau_s$ and P is required. This last relation is given by the well-known equation which establishes the carrier lifetime dependence of our SOA versus carrier density [15]:

$$\frac{1}{\tau_s} = A + B\bar{N} + C\bar{N}^2 \tag{5}$$

where A, B, and C, which are, respectively, the non-radiative, spontaneous and Auger recombination coefficients, are the only parameters that will have to be fitted from the experimental results.

Using Eq. (5) and the fact that we have proved that $\bar{N}/\tau_s$ and Γg can be considered as functions of P_0 only, we can finally obtain $\bar{N}$, $\Gamma a = \Gamma\frac{\partial g}{\partial \bar{N}}$, and $P_s = \frac{\hbar\omega}{a\tau_s}S_{guide}$ as functions of P_0. This permits one to replace Eqs. (1) and (2) by the following pair of equations:

$$\frac{\mathrm{d}P_0}{\mathrm{d}z} = P_0\big[-\gamma + \Gamma g(P_0)\big] \tag{6}$$

$$\frac{\mathrm{d}M}{\mathrm{d}z} = M\left\{-\gamma + \Gamma g(P_0)\left[1 - \frac{P_0/P_s(P_0)}{1 + P_0/P_s(P_0) - i\Omega\tau_s(P_0)}\right]\right\} \tag{7}$$

Eqs. (6) and (7) are then numerically solved and the microwave transfer function of the SOA, $S_{21} = \gamma_i\frac{M(L)}{M(0)}$, where γ_i are the insertion losses, is computed. The initial conditions are: $M(0) = \sqrt{\gamma_i}\frac{mP_{in}}{2}$, and $P_0(0) = \sqrt{\gamma_i}P_{in}$, with P_{in} the DC optical input power, and m the input modulation rate.

It is important to note that the recombination coefficients A, B and C are the only fitting parameters of our model. Once obtained from experimental data, since they are material constants, they are fixed for any other experimental conditions. The validity of this assumptions will be experimentally verified below with a commercially available SOA (InP/InGaAsP Quantum Well Booster Amplifier from COVEGA).

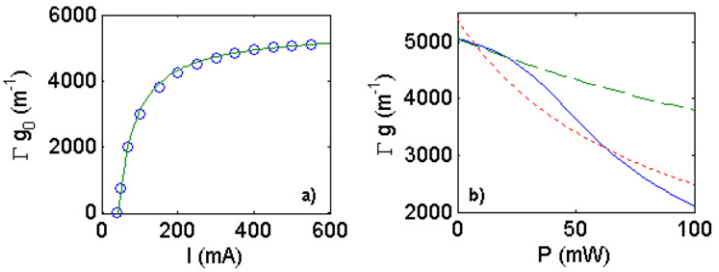

Fig. 1. (a) Experimental small signal gain Γg_0 as a function of the injected current I (circles). Solid line: empirical adjustment by: $\Gamma g_0 = C_1 - C_2/I$, with $C_1 = 5588.7\ \mathrm{m}^{-1}$ and $C_2 = 306.1\ \mathrm{A}^{-1}\,\mathrm{m}^{-1}$. (b) Material modal gain Γg as a function of the local DC power P_0 (solid line). In dashed lines: tentative adjustment by the material modal gain issued from usual models, $\Gamma \frac{g_0}{1+P_0/P_s}$, with g_0 and P_s constant: least squares adjustment (1) over the whole range, in red, $P_s = 85$ mW and $g_0 = 5400\ \mathrm{m}^{-1}$, and (2) over the small signal range, in green, $P_s = 300$ mW and $g_0 = 5055\ \mathrm{m}^{-1}$. (For interpretation of the references to color in this figure legend, the reader is referred to the web version of this article.)

Fig. 1. (a) Gain petit signal expérimental Γg_0, en fonction du courant injecté I, et interpolation empirique par : $\Gamma g_0 = C_1 - C_2/I$, avec $C_1 = 5588{,}7\ \mathrm{m}^{-1}$ et $C_2 = 306{,}1\ \mathrm{A}^{-1}\,\mathrm{m}^{-1}$. (b) Gain matériau modal expérimental $\Gamma g(\tilde{U})$ en fonction de l'intensité locale $\tilde{U}$ (trait plein), et les gains matériau modaux issus des modèles trouvés de littérature (en pointillés), $\frac{\Gamma g_0}{1+P/P_s}$, avec g_0 et P_s constants : ajustement par la méthode des moindres carrés (1) sur une grande plage d'intensités locales, en rouge, $P_s = 85$ mW et $g_0 = 5400\ \mathrm{m}^{-1}$, et (2) à faible puissance locale, en vert, $P_s = 300$ mW et $g_0 = 5055\ \mathrm{m}^{-1}$. (Pour l'interprétation des couleurs citées dans cette légende, le lecteur est prié de consulter la version web de cet article.)

2.2. *Experimental determination of the material modal gain $\Gamma g(P_0)$*

The preliminary step consists in measuring the unsaturated gain Γg_0 for different injected currents, in order to fully characterize the local gain response of the SOA through $\Gamma g(P_0)$ as described in Section 2.1. To get rid of the amplified spontaneous emission, the optical small signal gain is obtained by measuring the SOA unsaturated RF gain G_{RF} ($= |S_{21}|^2$) at low input optical power (typically 100 μW). In order to avoid possible RF gain saturation induced by coherent population oscillations, this measurement is conducted at 20 GHz RF-frequency, namely, well above $1/\tau_s$. Under these conditions, the optical small signal gain Γg_0 is expressed as:

$$\exp(\Gamma g_0 L) = \frac{\sqrt{G_{RF}}}{\gamma_i \exp(-\gamma L)}$$

The total losses of the SOA $\gamma_i \exp(-\gamma L)$ are obtained by an additional experimental measurement (−16.4 dB in our case). The unsaturated gain of our SOA is displayed in Fig. 1a. From this simple measurement, the material modal gain Γg is then known as a function of the local optical power $P_0(z)$ inside the SOA (Fig. 1b, in solid line).

In Fig. 1b, we also represent, in dashed lines, the material modal gain according to most practical models: $\Gamma \frac{g_0}{1+P/P_s}$, with g_0 and P_s constant. This last expression is a straightforward consequence of the assumption that the gain varies with the carrier density according to $g(\bar{N}) = a(\bar{N} - N_0)$, with a constant. It can be noticed that a least squares adjustment accurately matches the experimentally derived data only for a reduced range of optical powers (for instance, at low input optical power). However, for the whole power range, only an approximative adjustment can be obtained. As a consequence, one foresees that those practical models will have an accuracy range restricted to limited optical power variations, and therefore limited experimental conditions (device gain, saturation and carrier density levels). In particular, this kind of model might be more adapted to bulk SOAs or electro-absorption modulators, with not too strong carrier density, and hence gain. But they cannot predict the material modal gain for any initial conditions, when the local power varies too much, as it is the case in high carrier confinement quantum well or quantum dots structures. Our model, based on this simple experimental determination of the material modal gain, will fill in this gap, as we will show in the next section.

2.3. *Measurement of RF transfer function of the SOA — Comparison with theory*

The complex RF transfer function S_{21} of the SOA is measured using a Vector Network Analyzer (VNA) (set-up in Fig. 2). The corresponding RF gain, $20\log|S_{21}|$ and RF phase shift, $\arg(S_{21})$ are reported in Fig. 3, where the experimental data are plotted as a function of the modulation frequency Ω. In (a) and (b) are first plotted the experimental measurements for different injected currents I, whereas in (c) and (d) the input optical power is changed.

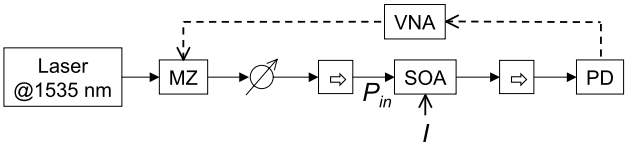

Fig. 2. Schematic representation of the experimental set-up A laser is externally modulated by a Mach–Zehnder modulator (MZ). The input optical power P_{in} is controlled through a variable optical attenuator. Two optical isolators are inserted at the input and output of the SOA in order to avoid any back-reflection. The photodetector (PD) converts the optical modulation into RF signal. The Vector Network Analyzer (VNA) is calibrated using, as a reference, the optical link without the SOA. The SOA is then inserted into the link and its RF transfer function is measured.

Fig. 2. Montage expérimental. Un modulateur externe permet de moduler l'intensité par le signal RF généré par le port 1 de l'analyseur de réseau (VNA). Des isolateurs sont placés avant et après le SOA. La puissance optique d'entrée P_{in} est contrôlée par un atténuateur variable. Le signal RF, restitué par la photodiode, est ensuite analysé par le VNA (port 2). Le VNA est calibré avec la liaison sans le SOA, afin de ne mesurer que la fonction de transfert du SOA.

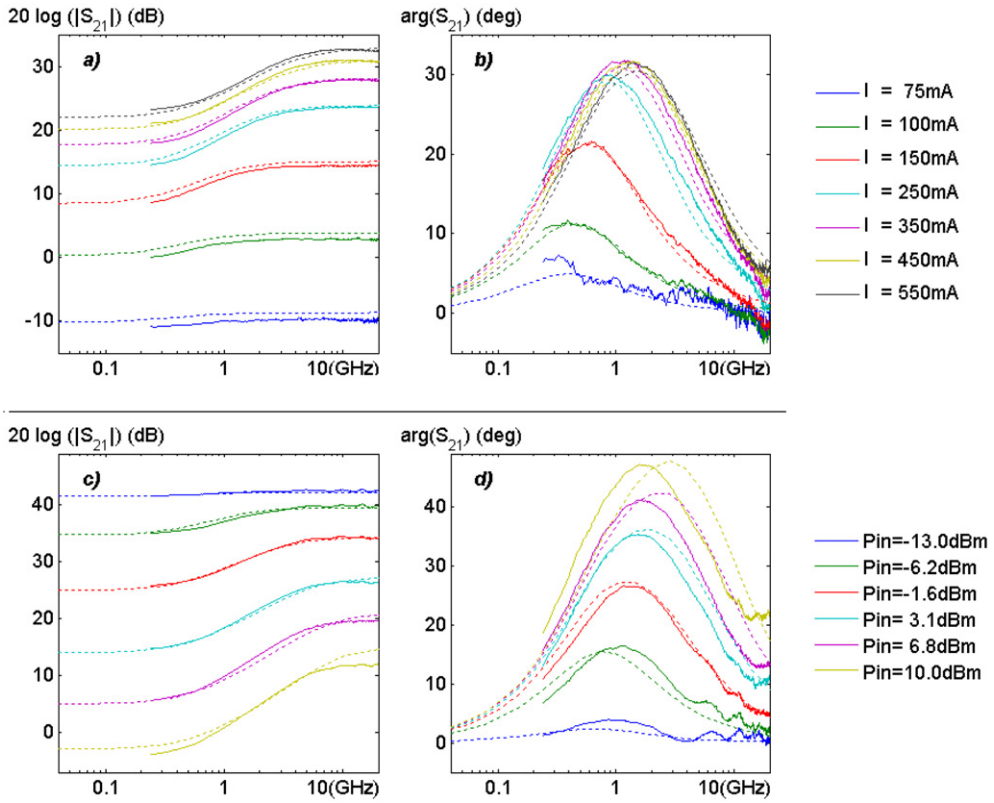

Fig. 3. Gain and phase shift simulations (dashed line) and experimental data (solid line) for (a) and (b): different injected currents I at $P_{in} = 0$ dBm, and for (c) and (d): different optical input powers P_{in} at $I = 500$ mA.

Fig. 3. Variations du gain et de la phase introduites par le SOA : données expérimentales (trait plein) et simulations (pointillés) pour (a) et (b) : différents courants injectés I à $P_{in} = 0$ dBm, et pour (c) et (d) : différentes puissances optiques d'entrée P_{in} à $I = 500$ mA.

In Fig. 3 are also represented the simulation results in dashed lines. The best fit values for the recombination coefficients are: $A = 2 \times 10^9\ \mathrm{s}^{-1}$, $B = 2 \times 10^{-10}\ \mathrm{cm}^3\,\mathrm{s}^{-1}$, $C = 5 \times 10^{-29}\ \mathrm{cm}^6\,\mathrm{s}^{-1}$. These values are in the range of those commonly found in the literature for InP/InGaAsP QW structures, the constitutive materials of our device [13,16,17]. The computed complex transfer function shows a very good agreement with the experimental data, either when the injection current or the input optical power is changed, which therefore proves the predictive capability of our model.

Consequently, we showed that the simple measurement of the small signal gain Γg_0 versus the injected current, enables to fully characterize the saturation dynamics for any injected current or optical power. The adjustable param-

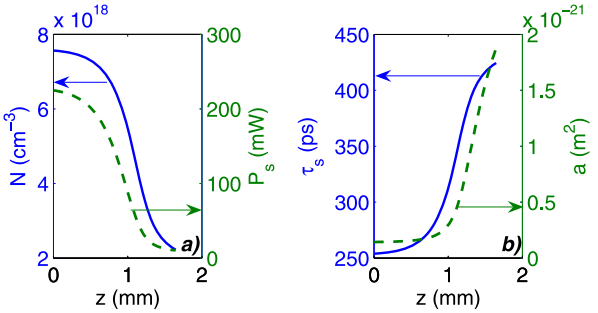

Fig. 4. Simulations for $P_{in} = 0$ dBm and $I = 500$ mA of (a) the carrier density $\bar{N}$ (solid line), and the local saturation power P_s (dashed line), along the SOA; (b) the carrier lifetime τ_s (solid line), and the modal differential gain $\tilde{a}$ (dashed line), along the SOA.

Fig. 4. Simulations pour $P_{in} = 0$ dBm et $I = 500$ mA de (a) la densité de porteurs $\bar{N}$ (trait plein), et de la puissance de saturation locale P_s (pointillés), suivant l'axe de propagation dans le SOA ; (b) le temps de vie des porteurs τ_s (trait plein), et le gain modal différentiel $\tilde{a}$ (pointillés), suivant l'axe de propagation dans le SOA.

eters are then reduced to the recombination coefficients A, B, C, which only depend on the material nature and/or characteristics. Once they are determined for a given SOA, we obtain a model which can accurately predict the RF complex transfer function of the SOA, for any experimental conditions.

Fig. 4 reproduces the evolution of the carrier density N along the SOA, and the subsequent variations of the saturation parameters P_s, τ_s an Γa. We find nearly one order of magnitude of variation for almost all these parameters, which are, nevertheless, all taken constant in previous practical models. Once again, according to (5), this approximation can be justified in the case of relatively low values of N, that is for a not too strong carrier confinement such as in bulk SOAs or electro-absorption modulators. However, this also reinforces the conclusion shown in this paper, that in the case of quantum well or quantum dots structures, it is necessary to take into account the saturation dynamics along the propagation to ensure the accuracy of the model and its robustness versus changes in experimental conditions.

At this stage, the present work thus enables to accurately predict the RF gain and phase shift produced by a semiconductor slow light element when injected current and input power are changed. It therefore gives the functional behavior of this element when integrated in a microwave photonics architecture. However, towards a real integration, it is also required to predict the impact of this device on the link performances. Consequently, in the next section, we will use our model of the RF transfer function to analyze the influence of slow light effect on noise properties and derive a practical predictive model for the relative intensity noise of the SOA.

3. Influence of slow light effect on noise properties

3.1. Model

In order to analyze the influence of slow light effect on the dynamic range of microwave-photonics links, the additional noise in SOAs has to be characterized. The noise is composed of the shot noise, the thermal noise and the relative intensity noise (RIN). The noise spectral density can then be written as:

$$\mathrm{DSP}_{noise} = RB_e\left(\mathrm{RIN}I_{ph}^2 + 2eI_{ph} + \frac{kT}{R}\right) \tag{8}$$

with RIN the relative intensity noise, I_{ph} the photodetected current, B_e the electrical bandwidth, R the photodetector load resistance, and T the temperature. The RIN has a specific behavior for SOAs, especially in slow light regime, which we propose to analyze in the following.

The relative intensity noise (RIN) is defined as:

$$\mathrm{RIN} = \frac{\langle \Delta I_{ph}^2 \rangle}{I_{ph}^2} \tag{9}$$

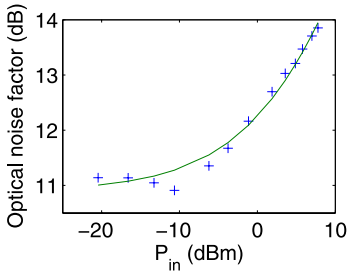

Fig. 5. Optical noise factor: experimental data and empirical fit $F = 12.3 \times \{1 + [0.072 \times P_{in}\ (\mathrm{mW})]^{0.570}\}$.

Fig. 5. Facteur de bruit optique : données expérimentales et ajustement empirique $F = 12{,}3 \times \{1 + [0{,}072 \times P_{in}\ (\mathrm{mW})]^{0{,}570}\}$.

where $\langle\,\rangle$ denotes time averaging. I_{ph} is the current of the photodetector, which can be expressed as a function of the total field E_{total} detected by the photodetector:

$$I_{ph} = \frac{e}{h\nu}\left\langle E_{total}^2 \right\rangle \tag{10}$$

where this time $\langle\,\rangle$ denotes an averaging on optical frequencies.

Our approach corresponds to the semi-classical beating theory. The output field of the SOA, E_{total}, is composed of the amplified input signal and the amplified spontaneous emission. Thus the noise density has two contributions, named as signal-spontaneous beat-note and spontaneous–spontaneous beat-note:

$$\left\langle \Delta I_{ph}^2 \right\rangle = S_{ASE\text{–}ASE} + S_{s\text{-}ASE} \tag{11}$$

where $S_{ASE\text{–}ASE}$ and $S_{s\text{-}ASE}$ are the spectral densities originating from the signal-spontaneous beat-note and the spontaneous–spontaneous beat-note, respectively.

In order to express these two contributions, we define the input spontaneous emission power density as the quantum noise source at the input of SOA [18]:

$$\rho_{in}^{noise} = \frac{h\nu}{2}\left(F - \frac{1}{G}\right) \tag{12}$$

with F the noise factor, and G the optical gain of the SOA.

Hence, the fields at the input of the SOA are the signal and the input quantum noise. The input intensity is composed of: (1) a signal-spontaneous beat-note, which can be considered as a sum of modulation components at the frequencies Ω: the response of the SOA is the microwave saturated gain of the SOA $|S_{21}(\Omega)|$; and (2) a spontaneous–spontaneous beat-note which is only responsive to the optical gain G.

Consequently, the noise output spectral densities are [19]:

$$S_{s\text{-}ASE}(\Omega) = 4\left|S_{21}(\Omega)\right|^2 \rho_{in}^{noise} P_{in}^{sig} B_e \tag{13}$$

$$S_{ASE\text{–}ASE}(\Omega) = 2G^2\left(\rho_{in}^{noise}\right)^2 B_0(1 - \Omega/B_0)B_e \tag{14}$$

with P_{in}^{sig} the input signal power in the SOA, B_0 the optical bandwidth before the photodetector, B_e the electrical bandwidth of the detection chain. Over the usual range of the microwave signal ($\ll$100 GHz), $S_{ASE\text{–}ASE}$ is independent of the frequency Ω. Consequently, only the s-ASE beat-note contributes to the frequency dependence of the noise output spectral densities, through $|S_{21}(\Omega)|^2$: the RIN is thus strongly linked to the slow light effect.

3.2. Experiment — Comparison with theory

The first step consists in measuring the noise factor F of the SOA in order to define ρ_{in}^{noise}. We used an optical method described in [18] to obtain the experimental data displayed in Fig. 5. The empirical fit of these data and the previous modeling of S_{21} developed in Section 2 are the only inputs of the RIN model. No additional parameters or adjustments are necessary.

The specific RIN of the SOA is measured thanks to the method described in [20]. The experimental data are displayed in Fig. 6. The simulations, also reported in Fig. 6, are in a very good agreement with measurements, once

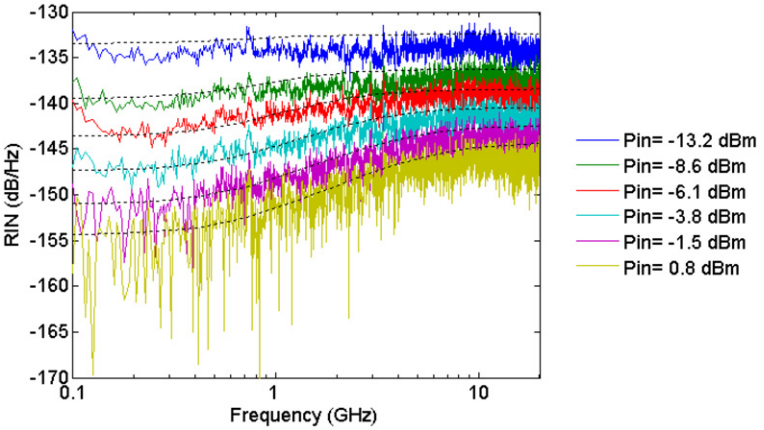

Fig. 6. Relative intensity noise (RIN): experimental and simulated data, respectively in solid line and dashed line.

Fig. 6. Bruit relatif d'intensité (RIN) : mesures (trait plein) et simulations (pointillés).

again with no additional adjustment. One can notice that according to (13), the dip experienced in the gain transfer function in the slow light regime, is reported on the RIN. This result forebodes that the dynamic range will be preserved even at low frequencies, where the slow light effect occurs. The predictive model of the RIN developed here will enable us to accurately study further the influence of the integration of SOAs on the dynamic range of the link.

4. Conclusion

We developed an improved model in order to predict the RF behavior and slow light properties of the SOA, valid for any experimental conditions (input optical power, injected current). It takes into account the dynamic saturation along the SOA, fully characterized by the simple measurement of the small signal gain, and only relies on material fitting parameters, independent of the optical intensity and bias current. We showed a remarkably good agreement between the model and the experimental data.

The ease of use and the accurate prediction obtained for any experimental conditions make this model a useful tool to characterize the effect of slow light in SOA on a microwave link. We already shown that it enables to fully describe the additive noise of the SOA. A future study will lead us to study the linear dynamic range of the SOA. Furthermore, in order to determine the harmonic generation, intermodulation products and spurious free dynamic range, a generalization of our approach (relying on the same experimental determination of the material modal gain) will be carried out in a next step, for a full characterization of a SOA based optoelectronic link.

Acknowledgements

The authors acknowledge the partial support from the GOSPEL European project and from the French "Délégation Générale pour l'Armement".

References

[1] J. Yao, Microwave photonics, J. Lightwave Technol. 27 (2009) 314–335.
[2] J. Capmany, B. Ortega, D. Pastor, A tutorial on microwave photonic filters, J. Lightwave Technol. 24 (2006) 201–229.
[3] D. Dolfi, et al., Experimental demonstration of a phased-array antenna optically controlled with phase and time delays, Appl. Opt. 35 (1996) 5293–5300.
[4] P.-C. Ku, et al., Slow light in semiconductor quantum wells, Opt. Lett. 29 (2004) 2291–2293.
[5] R. Boula-Picard, et al., Impact of the gain saturation dynamics in semiconductor optical amplifiers on the characteristics of an analog optical link, J. Lightwave Technol. 23 (2005) 2420–2426.
[6] J. Mørk, et al., Slow light in a semiconductor waveguide at gigahertz frequencies, Opt. Express 13 (2005) 8136–8145.
[7] S.S. Maicas, et al., Controlling microwave signals by means of slow and fast light effects in SOA-EA structures, IEEE Photon. Technol. Lett. 19 (2007) 1589–1591.

[8] Y. Chen, J. Mørk, Broadband microwave phase shifter based on high speed cross gain modulation in quantum dot semiconductor optical amplifiers, in: International Topical Meeting on Slow and Fast Light, in: 2009 OSA Technical Digest, Optical Society of America, 2009.
[9] G.P. Agrawal, Population pulsations and nondegenerate four-wave mixing in semiconductor lasers and amplifiers, J. Opt. Soc. Am. B 5 (1988) 147–159.
[10] S.-W. Chang, et al., Slow light based on coherent population oscillation in quantum dots at room temperature, IEEE J. Quantum Electron. 43 (2007) 196–205.
[11] A. Capua, et al., Direct observation of the coherent spectral hole in the noise spectrum of a saturated InAs/InP quantum dash amplifier operating near 1550 nm, Opt. Express 16 (2008) 2141–2146.
[12] J. Kim, et al., Static gain saturation model of quantum-dot semiconductor optical amplifiers, IEEE J. Quantum Electron. 44 (2008) 658–666.
[13] M.J. Connelly, Wideband semiconductor optical amplifier steady-state numerical model, IEEE J. Quantum Electron. 37 (2001) 439–447.
[14] H. Su, S.L. Chuang, Room temperature slow and fast light in quantum-dot semiconductor optical amplifiers, Appl. Phys. Lett. 88 (2006) 061102.
[15] L.A. Coldren, S.W. Corzine, Diode Lasers and Photonic Integrated Circuits, Wiley & Sons, 1995.
[16] E. Rosencher, B. Vinter, Optoelectronics, Cambridge, 2002.
[17] A. Haug, Evidence of the importance of Auger recombination for InGaAsP lasers, Electron. Lett. 20 (1984) 85–86.
[18] D.M. Baney, P. Gallion, R.S. Tucker, Theory and measurement techniques for the noise figure of optical amplifiers, Opt. Fiber Technol. 6 (2000) 122–154.
[19] N.A. Olsson, Lightwave systems with optical amplifiers, J. Lightwave Technol. 7 (1989) 1071–1082.
[20] G. Baili, et al., Shot-noise-limited operation of a monomode high-cavity-finesse semiconductor laser for microwave photonics applications, Opt. Lett. 32 (2007) 650–652.